

Structure of ground and excited states of ^{12}C

Y. Kanada-En'yo

*Yukawa Institute for Theoretical Physics, Kyoto University,
Kyoto 606-8502, Japan*

We studied the ground and excited states of ^{12}C based on variational calculations after spin-parity projection in a framework of antisymmetrized molecular dynamics(AMD). The calculations systematically reproduce various experimental data. It was found that the sub-shell closure and $SU(3)$ -limit 3α cluster components are contained in the ground state, while various 3α cluster structures develop in the excited states. We discussed effects of α breaking and show the importance of coexistence of the cluster and shell-model-like aspects.

I. INTRODUCTION

The formation of mean-field is an important aspect in nuclear systems. It results in the shell-model-like nature of nuclear structure. On the other hand, in a region of light nuclei, it is well known that clustering is another essential feature. These two different kinds of nature, cluster and shell-model-like aspects, often coexist, compete and interplay between each other. The coexistence of two aspects provides a variety of structure in nuclear systems, and can be a key to reveal properties of light nuclei.

^{12}C is one of the typical examples where the cluster and shell-model-like aspects coexist. Since ^{12}C is the double sub-shell closure of the $p_{3/2}$ shell in the j - j coupling picture, the ground state should contain such the shell-model-like nature. On the other hand, 3α -cluster structure is also favored in ^{12}C and is considered to develop in excited states. Shell model calculations succeeded to reproduce experimental data of many levels in light nuclear region(for example, [1,2]). However, a number of states in light nuclei have been left unsolved in those shell model studies because it is difficult for the shell models to describe well-developed cluster states in general. In fact, even the large basis shell model calculations failed to describe such the excited states as the 0_2^+ state at $E_x = 7.65$ MeV and the 3_1^- state at $E_x = 9.64$ MeV near the 3α threshold energy [3]. These states have been considered to be well-developed cluster states, and their structures have been studied with 3α cluster models for a long time [4–8]. Recently, Tohsaki *et al.* proposed a new interpretation of the 0_2^+ state as a dilute cluster gas state of weakly interacting 3 α particles [9], and discussed it in the relation with the Bose Einstein Condensed(BEC) phase in dilute nuclear matter [10]. Moreover, there are many experimental reports on the resonances in the excitation energy region around $E_x = 10$ MeV recently [11–14]. Especially, the experimentally suggested 0^+ and 2^+ states in the broad resonances at $E_x \sim 10$ MeV attract an interest because these states are the candidates of the well-developed cluster states. Although the structure of these resonances [15–18] has been theoretically studied based on the 3α cluster model approaches, their properties have not been clarified yet. The cluster model approaches are useful to describe the details of inter-cluster motion in the 3α system, however, they failed to reproduce such the data as the excitation energy of the 2_1^+ and the strengths of β decays, because these properties are sensitive to such the shell-model-like features as the sub-shell closure and the α breaking of ^{12}C but the 3α -cluster models is not suitable for describing the j - j coupling features nor dissociation of the α clusters.

These facts indicate that the cluster and shell-model-like features certainly coexist in the ^{12}C system. It is expected that the shell-model-like aspects in the low-lying states may have some influence on the excited cluster states through the orthogonality and mixing with the lower states. Therefore, it is important to take into account both aspects in the systematic study of ^{12}C . However, there are a few theoretical studies of ^{12}C where both the cluster and the shell-model-like features are taken into account. The method of antisymmetrized molecular dynamics(AMD) has been proved to be a powerful approach to describe the cluster and shell-model-like features in general nuclei. Since all the single-nucleon wave functions are treated as independent Gaussian wave packets in this method, the existence of clusters are not assumed in the model. Instead, if the system favors a cluster structure, the cluster state automatically appears in the energy variation in this framework. For the excited states, the method of variation after spin-parity projection(VAP) in the framework of AMD is a useful approach [19–21]. The author has performed the first VAP calculations of AMD and briefly reported its application to ^{12}C [19]. Itagaki *et al.* also have investigated the cluster and shell competition in the ^{12}C system while incorporating the dissociation of α clusters [22]. However, the work was limited to the low-lying states. Neff *et al.* have done the VAP calculations within the fermionic molecular dynamics(FMD) [23], which is similar approach to the AMD. Although the FMD wave function is suitable for describing both the cluster and shell-model-like structures in principle as well as the AMD, the existence of 3 α -clusters were *a priori* assumed in the practical application to ^{12}C in [23].

In the present work, we studied the structure of the ground and excited states of ^{12}C with the method of the VAP in the AMD framework. The method is almost the same as that applied in our previous work [19]. We calculated various quantities such as radii, transition strengths and densities, and compared them with the experimental data and other theoretical calculations. The structures of the ground and excited states were analyzed while focusing on the cluster structure and the dissociation of the α clusters. We also estimated the partial decay widths of the resonances with the method of reduced with amplitudes.

This paper is organized as follows. In II, we give a brief explanation of the formulation of the present work. The adopted effective nuclear interactions are described in III. In IV, we show the calculated results concerning such observables as the energy levels, radii and β decays as well as the $E0$ and $E2$ transitions compared with the experimental data. In an analysis of the obtained wave functions in V), the shell-model-like and cluster features are discussed. In the last section(VI), we give a summary.

II. FORMULATION

The detailed formulation of the AMD method for nuclear structure studies is described in [19,20,24–26]. In particular, the formulation of the present calculations is basically the same as that described in [19–21].

An AMD wave function is a Slater determinant of Gaussian wave packets;

$$\Phi_{\text{AMD}}(\mathbf{Z}) = \frac{1}{\sqrt{A!}} \mathcal{A}\{\varphi_1, \varphi_2, \dots, \varphi_A\}, \quad (1)$$

where \mathcal{A} is the antisymmetrizer and A is the mass number. The i -th single-particle wave function is written by a product of spatial(ϕ), intrinsic spin(χ) and isospin(τ) wave functions as,

$$\varphi_i = \phi_{\mathbf{X}_i} \chi_i \tau_i, \quad (2)$$

$$\phi_{\mathbf{X}_i}(\mathbf{r}_j) \propto \exp\left\{-\nu\left(\mathbf{r}_j - \frac{\mathbf{X}_i}{\sqrt{\nu}}\right)^2\right\}, \quad (3)$$

$$\chi_i = \left(\frac{1}{2} + \xi_i\right)\chi_{\uparrow} + \left(\frac{1}{2} - \xi_i\right)\chi_{\downarrow}. \quad (4)$$

The spatial part is represented by complex variational parameters, \mathbf{X}_{1i} , \mathbf{X}_{2i} , \mathbf{X}_{3i} , which indicate the center of the Gaussian wave packet. The orientation of the intrinsic spin is expressed by a complex variational parameter ξ_i , and the isospin function is fixed to be up(proton) or down(neutron). We used a common value of the width parameter ν , which is chosen to be the optimum value of each nucleus. Accordingly, an AMD wave function is expressed by a set of variational parameters, $\mathbf{Z} \equiv \{\mathbf{X}_1, \mathbf{X}_2, \dots, \mathbf{X}_A, \xi_1, \xi_2, \dots, \xi_A\}$.

We performed the energy variation after spin-parity projection(VAP) in the AMD model space. In order to obtain the wave function for the lowest J^π state, we varied the parameters \mathbf{X}_i and ξ_i ($i = 1 \sim A$) to minimize the energy expectation value of the Hamiltonian, $\langle \Phi | H | \Phi \rangle / \langle \Phi | \Phi \rangle$, for the spin-parity projected AMD wave function; $\Phi = P_{MK'}^{J\pi} \Phi_{\text{AMD}}(\mathbf{Z})$. $P_{MK'}^{J\pi}$ is the spin-parity projection operator. By the VAP calculation for the J^π eigen state with an appropriate K' , we first obtained a set of parameters $\mathbf{Z} = \mathbf{Z}_1^{J\pi}$ for the lowest J^π state which is expressed by $P_{MK'}^{J\pi} \Phi_{\text{AMD}}(\mathbf{Z}_1^{J\pi})$. In order to search for the parameters \mathbf{Z} for the higher J^π state, the VAP is performed in the orthogonal space to the lower states. The parameters $\mathbf{Z}_n^{J\pi}$ for the n th J^π state are provided by varying \mathbf{Z} so as to minimize the energy of the wave function;

$$|\Phi\rangle = |P_{MK'}^{J\pi} \Phi_{\text{AMD}}(\mathbf{Z})\rangle - \sum_{k=1}^{n-1} |P_{MK'}^{J\pi} \Phi_{\text{AMD}}(\mathbf{Z}_k^{J\pi})\rangle \frac{\langle P_{MK'}^{J\pi} \Phi_{\text{AMD}}(\mathbf{Z}_k^{J\pi}) | P_{MK'}^{J\pi} \Phi_{\text{AMD}}(\mathbf{Z}) \rangle}{\langle P_{MK'}^{J\pi} \Phi_{\text{AMD}}(\mathbf{Z}_k^{J\pi}) | P_{MK'}^{J\pi} \Phi_{\text{AMD}}(\mathbf{Z}_k^{J\pi}) \rangle}, \quad (5)$$

which is orthogonalized to the lower states.

After the VAP calculation of the J_n^π states for various J , n and $\pi = \pm$, we obtained the optimum intrinsic states, $\Phi_{\text{AMD}}(\mathbf{Z}_n^{J\pi})$, which approximately describe the corresponding J_n^π states. In order to improve the wave functions, we superposed all the obtained AMD wave functions. Namely, we determined the final wave functions for the J_n^π states by simultaneously diagonalizing the Hamiltonian matrix, $\langle P_{MK'}^{J\pi} \Phi_{\text{AMD}}(\mathbf{Z}_{n_i}^{J_i \pi_i}) | H | P_{MK''}^{J\pi} \Phi_{\text{AMD}}(\mathbf{Z}_{n_j}^{J_j \pi_j}) \rangle$, and the norm matrix, $\langle P_{MK'}^{J\pi} \Phi_{\text{AMD}}(\mathbf{Z}_{n_i}^{J_i \pi_i}) | P_{MK''}^{J\pi} \Phi_{\text{AMD}}(\mathbf{Z}_{n_j}^{J_j \pi_j}) \rangle$, with respect to (i, j) for all of the obtained intrinsic states and (K', K'') . Consequently, the J_n^π state are written as,

$$|J_n^\pi\rangle = \sum_{i,K} c(J_n^\pi, i, K) |P_{MK}^{J\pi} \Phi_{\text{AMD}}(\mathbf{Z}_{k_i}^{J_i \pi_i})\rangle, \quad (6)$$

where the coefficients $c(J_n^\pi, i, K)$ are determined by the diagonalization of the Hamiltonian and norm matrices. In comparison of theoretical values with the experimental data, we calculated the expectation values for the corresponding operators by the $|J_n^\pi\rangle$.

III. INTERACTIONS AND PARAMETERS

The effective nuclear interaction adopted in the present work consists of the central force, the spin-orbit force and the Coulomb force. We adopted MV1 force [27] as the central force, which contains a zero-range three-body force in addition to the two-body interaction. Concerning the spin-orbit force, the same form of the two-range Gaussian as the G3RS force [28] is adopted. The adopted interaction parameters are the same as those used in the previous work [19]. Namely, the Bartlett, Heisenberg and Majorana parameters in the MV1 force are chosen to be $b = h = 0$ and $m = 0.62$, and the strengths of the spin-orbit force are taken to be $u_I = -u_{II} = 3000$ MeV.

We used the width parameter $\nu = 0.19$ fm⁻² for the single-particle Gaussian wave packets in Eq. 3 so as to minimize the energy of the lowest 0^+ state.

In the previous work [19], we situated an artificial barrier potential in the procedure of the energy variation to confine nucleons within the inner region in the same way as Ref. [20]. Since we are interested in the dilute cluster states, we performed the energy variation without the barrier potential. We also did the variation with the barrier potential and combined the obtained wave functions as the base wave functions in the diagonalization of Hamiltonian and norm matrices.

IV. RESULTS

The wave functions of the ground and excited states of ¹²C were calculated based on the VAP calculations in the framework of AMD. In this section, we show theoretical results and compare them with experimental data.

The wave functions for the lowest J^π states were obtained by the VAP calculation of $P_{MK'}^{J^\pi} \Phi_{\text{AMD}}$ by using $(J^\pi, K') = (0^+, 0), (2^+, 0), (4^+, 0), (6^+, 0), (1^-, 1), (2^-, 1), (3^-, 3), (4^-, 3), (5^-, 3), (1^+, 0)$. After obtaining the lowest states (J_1^π), we calculated the second and third J^π states ($0_2^+, 0_3^+, 2_2^+, 2_3^+, 4_2^+$) with the VAP calculation in the model space orthogonal to the obtained lower J^π states.

Those VAP calculations were performed without the artificial barrier potential. As shown later, thus obtained intrinsic wave functions for the $0_3^+, 2_2^+, 2_3^+, 4_2^+, 6_1^+, 1_1^-, 2_1^-$ states are not compact states but spatially expanded states where α particles distribute far away from the center. For these states, we also performed the VAP calculations with the artificial barrier potential [20] in the same way as the previous work [19] to keep the particles in an intermediate distance region.

The obtained AMD wave functions ($\Phi_{\text{AMD}}(\mathbf{Z}_n^{J^\pi})$) are considered to approximately describe the intrinsic states of the corresponding J_n^π states. The final wave functions of the J_n^π states were determined by superposing the spin-parity eigen states projected from these obtained AMD wave functions so as to simultaneously diagonalize the Hamiltonian and the norm matrices. For the 1^+ state, we found that the obtained wave function, $P_{M1}^{1+} \Phi_{\text{AMD}}(\mathbf{Z}^{1+})$, contains a significant isospin breaking component. Therefore, we added the mirror wave function $P_{p \leftrightarrow n} P_{M1}^{1+} \Phi_{\text{AMD}}(\mathbf{Z}^{1+})$ of the original one to the set of base AMD wave functions in the diagonalization. Here $P_{p \leftrightarrow n}$ is the proton-neutron exchange operator. As a result, the number i of the superposed AMD wave functions $P_{MK'}^{J^\pi} \Phi_{\text{AMD}}(\mathbf{Z}_{n_i}^{J_i \pi_i})$ is 23 in the present calculations.

A. Energies

The theoretical binding energy of ¹²C is 88.0 MeV. Although the calculation slightly underestimates the experimental value 92.16 MeV, it can be improved by changing the Majorana parameter m of the interaction.

In Fig. 1, the energy levels of the present results (AMD) are shown with the experimental data and the other calculations of 3α cluster models; the resonating group method (RGM) [4] with the Volkov No.2 force and the generator coordinate method (GCM) [6] with the Volkov No.1 force. Recently, further theoretical works were performed based on 3α cluster models, where resonant 3α states were treated in more details [15–18]. The energy spectra obtained in these works are almost consistent with either of the 3α RGM [4] and 3α GCM [6] results shown in Fig. 1, except for the new broad $0+$ state predicted in [16].

In the ground band, the AMD calculation reproduces well the level spacing between 0_1^+ and 2_1^+ , while all the 3α calculations underestimate it. The success of the AMD is owing to the energy gain of the spin-orbit force in the 0_1^+

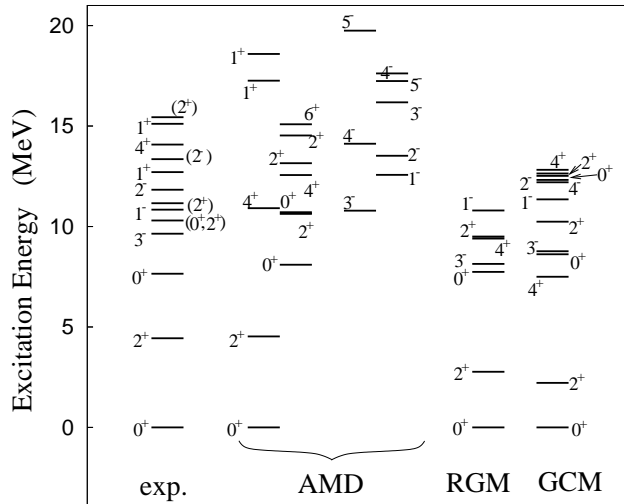


FIG. 1. Energy levels of the ground and excited states of ^{12}C . The theoretical levels of the $3\alpha\text{RGM}$ and $3\alpha\text{GCM}$ are the results of [4] and [6], respectively.

with the breaking of the 3α clustering. In other words, this large level spacing is one of the characteristics of the $p_{3/2}$ sub-shell closure, which can not be described within the 3α cluster models.

For the positive parity states with natural spins above the 3α threshold energy (7.272 MeV), the 0_2^+ , 0_3^+ , 2_2^+ , 2_3^+ , 4_1^+ , 4_2^+ and 6_1^+ states are obtained in the AMD results. The level structure of these states is similar to that of the $3\alpha\text{GCM}$ calculations [6]. Since the highly excited states, 0_3^+ , 2_2^+ , 2_3^+ and 6_1^+ , have the dominant component with an α -particle far from the other two α 's, the stability of these states should be analyzed by treating the boundary condition of the resonant states carefully.

The level spectra of the positive parity states around $E_x = 10 \sim 11$ MeV and their properties have not been clarified experimentally and theoretically. In the AMD results, the 0_3^+ state appears at 3 MeV higher energy than the 0_2^+ state. The 0_3^+ state was predicted also in the $3\alpha\text{GCM}$ calculation [6], while Kurokawa *et al.* proposed a new broad 0^+ state below the 0^+ in the recent work with the method of analytic continuation in the coupling constant combined with the complex scaling method (ACCC+CSM) [16]. As discussed later, the 0_3^+ in the present result corresponds to the 0_3^+ state of the $3\alpha\text{GCM}$ calculation. The detailed assignment of the excited states is discussed in the next section.

We obtain the 1_1^+ and 1_2^+ states. These states correspond to the $1^+(T=0)$ at 12.7 MeV and the $1^+(T=1)$ at 15.1 MeV. Since the spin-parity 1^+ is unnatural in a 3α system, it is difficult to describe these states within 3α cluster models. In fact, the present 1^+ states have the non- 3α component. The excitation energies of the 1^+ states are overestimated in the present results. They can be improved by tuning the strength of Bartlett and Heisenberg terms. For example, by using the interaction parameters, $b = h = 0.2$ and $m = 0.62$, we obtained the excitation energy $E_x(1_1^+) = 13.9$ MeV.

In the negative parity states, we obtained $\{3_1^-, 4_1^-, 5_2^-\}$ and $\{1_1^-, 2_1^-, 3_2^-, 4_2^-, 5_1^-\}$, which construct the rotational bands, $K = 3^-$ and $K = 1^-$, respectively. These bands are consistent with the $3\alpha\text{GCM}$ calculations.

B. Radii

The theoretical values of the root mean square radius (R_m) of mass distributions are shown in Table I. The calculated radius of the ground state is $R_m = 2.53$ fm, which is slightly larger than other 3α calculations and is large compared with the observed value $R_m = 2.32 - 2.33$ fm deduced from the charge radius. The radii (R_m) of the excited states in the present results seem to be qualitatively consistent with the those of the $3\alpha\text{GCM}$ calculations.

Recently, the structure of the 0_2^+ state attracts a great interest, because Tohsaki *et al.* [9] proposed a new interpretation of the 0_2^+ as a dilute α -cluster gas, where weakly interacting 3 α 's form an α condensate state. In their work, the 0_2^+ has the extremely large radius because of its dilute 3α gas-like structure. Although the radius of the 0_2^+ is somewhat smaller in the present result than the theoretical values of the 3α calculations, it is still remarkably large compared with that of the ground state. In the present framework, the long tail of the inter-cluster wave functions at a dilute density may be underestimated because the base AMD wave functions is limited to only 23 Slater determinants obtained by the VAP. We think that the dissociation of the α clusters can be another reason for the smaller radius

TABLE I. Root mean square radius for mass distributions. The theoretical values of the 3α -cluster calculations [4,6,17] are also listed. The values for the 3α condensate wave functions in Ref. [17] are those obtained with the Volkov No.2 force. The mass radii(R_m) for the 3α RGM calculations [4] are deduced from the charge radii(R_c) with the relation $R_c^2 = R_m^2 - R_p^2$, where R_p is the proton charge radius 0.813 fm. The observed charge radius of the ground state is $R_c = 2.46 - 2.47$ fm [29], which corresponds to $R_m = 2.32 - 2.33$ fm.

J^π	mass radius (fm)			
	present(AMD)	3α GCM [6]	3α RGM [4]	Funaki <i>et al.</i> [17].
0_1^+	2.53	2.40	2.40	2.40
0_2^+	3.27	3.40	3.47	3.83
0_3^+	3.98	3.52		
1_1^+	2.47			
1_2^+	2.47			
2_1^+	2.66	2.36	2.38	2.38
2_2^+	3.99	3.52	4.0	
2_3^+	3.50	3.34		
2_4^+	3.86			
4_1^+	2.71	2.29	2.31	2.31
4_2^+	4.16	3.64		
1_1^-	3.42	3.29	3.36	
2_1^-	3.49	3.32		
3_1^-	3.13	2.83	2.76	
3_2^-	3.56			
4_1^-	3.19	2.87		
4_2^-	3.53			

of the 0_2^+ than the 3α calculations. One of the origins of the dilute character of the 0_2^+ state is the orthogonality to the ground state. In the 3α cluster model, the ground state has the compact 3α wave function, the wave function of the 0_2^+ state tends to avoid overlapping with the compact 3α state to keep the orthogonality. However, in the present results, the ground state contains the α breaking component as naturally expected in the $p_{3/2}$ sub-shell closed nucleus. Due to the non- 3α component, the compact 3α wave function is partially allowed to mix into the 0_2^+ state, and it may reduce the size of the 0_2^+ state.

In Fig. 2, the matter density distributions are shown. The 0_1^+ , 2_1^+ and 4_1^+ in the ground band have compact density distributions. The density distributions of the 1^+ states are also compact and its radius is small because of the shell-model-like structure with the dominant $0\hbar\omega$ components as well as the ground state. In the 0_2^+ state, the density is suppressed in the small r region and spreads to the outer region. The shapes of the densities in the 0_3^+ , 2_2^+ and 4_2^+ are similar to each other. They have long tails due to the 3α linear-like structure. In the 3_1^- and 4_1^- states, the density at the center $r = 0$ fm is small, and the positions of the maximum density are large as $r \sim 1.5$ fm compared with those in other states because of a developed triangle 3α cluster structure.

C. $E2$ and $E0$ transitions

The $E2$ and $E0$ transition strengths are listed in Table II. The present $B(E2; 2_1^+ \rightarrow 0_1^+)$ value for the transitions in the ground band well agrees with the experimental data and is consistent with other theoretical calculations. For the transition between the 2_1^+ and the 0_2^+ , the 3α cluster calculations [6,4] usually underestimate the observed data by factor $2 \sim 4$. In the present results, the $B(E2; 2_1^+ \rightarrow 0_2^+)$ value is larger than those of the 3α calculations. It is because the spatial extension of the 3α distribution in the 0_2^+ is not so remarkable as the 3α calculations due to the α breaking component of the ground state, and can have a significant transition overlap with the 2_1^+ state. It means that the α breaking component affect the $B(E2; 2_1^+ \rightarrow 0_2^+)$ as argued in the work with the $\alpha + 4p + 4n$ model by Itagaki *et al.* [22]. Considering that the present result overestimates the observed $B(E2; 2_1^+ \rightarrow 0_2^+)$, the α breaking effect might be somewhat too strong. In the $E2$ transitions from the highly excited states such as the 2_2^+ , 0_3^+ , 4_2^+ , we obtained remarkably large $B(E2)$ values, $B(E2; 2_2^+ \rightarrow 0_2^+) = 100 \text{ e}^2\text{fm}^4$, $B(E2; 2_2^+ \rightarrow 0_3^+) = 310 \text{ e}^2\text{fm}^4$ and $B(E2; 4_2^+ \rightarrow 2_2^+) = 600 \text{ e}^2\text{fm}^4$, due to the large intrinsic deformation of the developed 3α cluster states. Since the $E2$ transitions $2_2^+ \rightarrow 0_3^+$ and $4_2^+ \rightarrow 2_2^+$ are especially strong, we consider that those are the intra-band transitions among the band members $\{0_3^+, 2_2^+$ and $4_2^+\}$. This assignment of the band members is also consistent with the similarity of

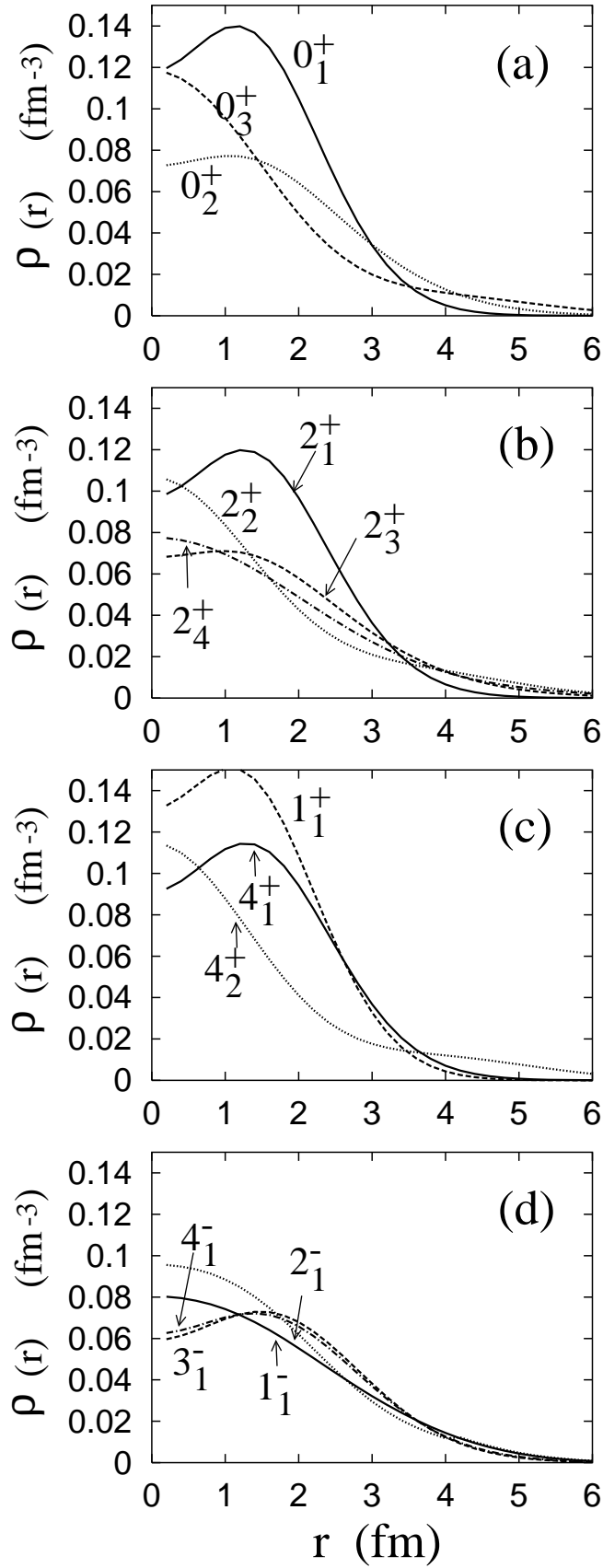


FIG. 2. Calculated matter density plotted as a function of radius r .

TABLE II. Strengths of $E2$ and $E0$ transitions. The experimental data are taken from Ref. [32]. The theoretical results of 3α GCM [6], 3α RGM [4] and $\alpha + 4p + 4b$ calculations [22] are also listed.

transitions	present(AMD)	3α GCM [6]	3α RGM [4]	$\alpha + 4p + 4n$ [22]	exp.
$B(E2; 2_1^+ \rightarrow 0_1^+)$	8.5	8.0	9.3	7.1	$7.6 \pm 0.4 e^2 \text{fm}^4$
$B(E2; 2_1^+ \rightarrow 0_2^+)$	5.1	0.7	1.1	2.8	$2.6 \pm 0.4 e^2 \text{fm}^4$
$B(E2; 2_2^+ \rightarrow 0_2^+)$	100				
$B(E2; 2_2^+ \rightarrow 0_3^+)$	310				
$B(E2; 2_3^+ \rightarrow 0_2^+)$	6.4				
$B(E2; 2_3^+ \rightarrow 0_3^+)$	76				
$B(E2; 4_1^+ \rightarrow 2_1^+)$	16				
$B(E2; 4_1^+ \rightarrow 2_2^+)$	7.5				
$B(E2; 4_2^+ \rightarrow 2_2^+)$	600				
$B(E2; 4_2^+ \rightarrow 2_3^+)$	74				
$M(E0; 0_1^+ \rightarrow 0_2^+)$	6.7	6.6	6.7		$5.4 \pm 0.2 \text{ fm}^2$
$M(E0; 0_2^+ \rightarrow 0_3^+)$	2.0				

the density form among these three states(see Fig. 2). The detailed discussion of the band structure is given in the next section.

The $E2$ transition densities $\rho_{J_f, J_i}^{(\lambda=2)}(r)$ are shown in Fig. 3. The density is normalized as,

$$B(E2; J_i \rightarrow J_f) = \frac{1}{2J_i + 1} \int r^4 dr \rho_{J_f, J_i}^{(\lambda=2)}(r). \quad (7)$$

The shapes of the transition densities for $2_1^+ \rightarrow 0_1^+$, $2_2^+ \rightarrow 0_1^+$, and $2_2^+ \rightarrow 0_2^+$ in the present results are consistent with those of the 3α RGM calculations [4]. The transition density for $2_1^+ \rightarrow 0_2^+$ has a significant strength in the region $r = 2 \sim 3$ fm in the present results, while, in the 3α RGM case, it has a node which suppresses $B(E2)$.

The elastic form factor for the ground state is shown in Fig. 4 (a). The dip position shifts toward the small q region compared with the observed data, because the present calculation overestimates the radius of the ground state as shown in Table I. The inelastic form factors for the electric monopole transitions, $0_1^+ \rightarrow 0_2^+$ and $0_1^+ \rightarrow 0_3^+$ are shown in Fig. 4(b). The first peak of the form factor for $0_1^+ \rightarrow 0_2^+$ well agrees with the observed data for the inelastic scattering into the 0_2^+ state at 7.65 MeV. The second peak at the high q region is smaller than the observed data because the calculation underestimates the observed elastic form factor of the ground state in this region. Recently, Funaki *et al.* discussed the dependence of the inelastic form factor on the nuclear size of the 0_2^+ within the 3α cluster model [30]. They argued that the maximum value of the form factor depends on the size. If the 0_2^+ state with the 3α structure has a small size, the inelastic form factor becomes large because of the large transition overlap with the compact ground state. In their analysis the observed form factor is well reproduced by the α condensate wave function with the radius $R_m = 3.8$ fm. Also in the 3α GCM and 3α RGM calculations, the form factor is well reproduced by the 0_2^+ with $R_m = 3.5$ fm. On the other hand, although the size of the 0_2^+ is as small as 3.3 fm in the present results, the maximum peak height of the calculations is in good agreement with that of the observed inelastic form factor. In the present case, the α breaking component in the ground state suppresses the transition into the 3α cluster state, because the non- 3α component has a small transition overlap with the 3α cluster state. It means that the absolute value of the inelastic form factor is not sensitive only to the size of the 0_2^+ state, but also depends on the α breaking component in the ground state.

The calculated form factor for the $0_1^+ \rightarrow 0_3^+$ has a similar q dependence to that of the $0_1^+ \rightarrow 0_2^+$. Its magnitude is one order smaller than for the $0_1^+ \rightarrow 0_2^+$ in the present results. It corresponds to the 3 times smaller transition matrix $M(E0; 0_1^+ \rightarrow 0_3^+) = 2.0 \text{ fm}^2$ than the $M(E0; 0_1^+ \rightarrow 0_2^+) = 6.0 \text{ fm}^2$. The isoscalar monopole strengths to the 0_2^+ and the 0_3^+ were studied by inelastic ${}^6\text{Li}$ and α scattering [11,31]. From the isoscalar energy weighted sum rule strength in those studies, the ratio $B(E0; 0_1^+ \rightarrow 0_3^+)/B(E0; 0_1^+ \rightarrow 0_2^+)$ is deduced to be $0.3 \sim 1$ by assuming the mirror symmetry. The present form factor for the $0_1^+ \rightarrow 0_3^+$ is smaller than these experimental values. In the 3α GCM calculations [6], the inelastic form factor for $0_1^+ \rightarrow 0_3^+$ is as large as that for $0_1^+ \rightarrow 0_2^+$ and is consistent with the observed data. In order to study the detailed structure of the 0_3^+ state, more precise experimental data are required.

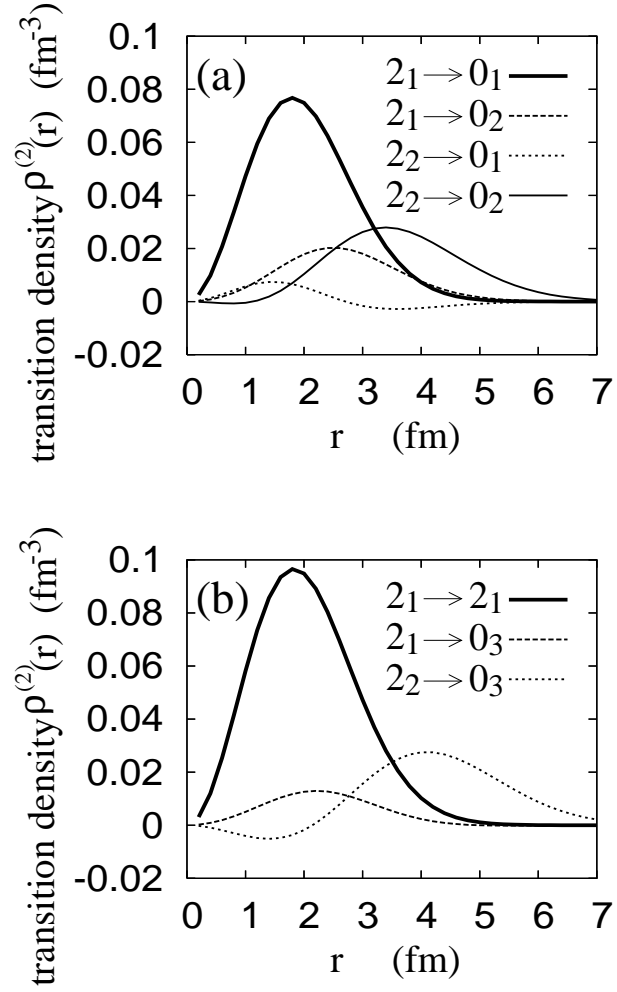


FIG. 3. Calculated $E2$ transition densities $\rho_{J_f, J_i}^{(\lambda=2)}(r)$ between the 0^+ and 2^+ states.

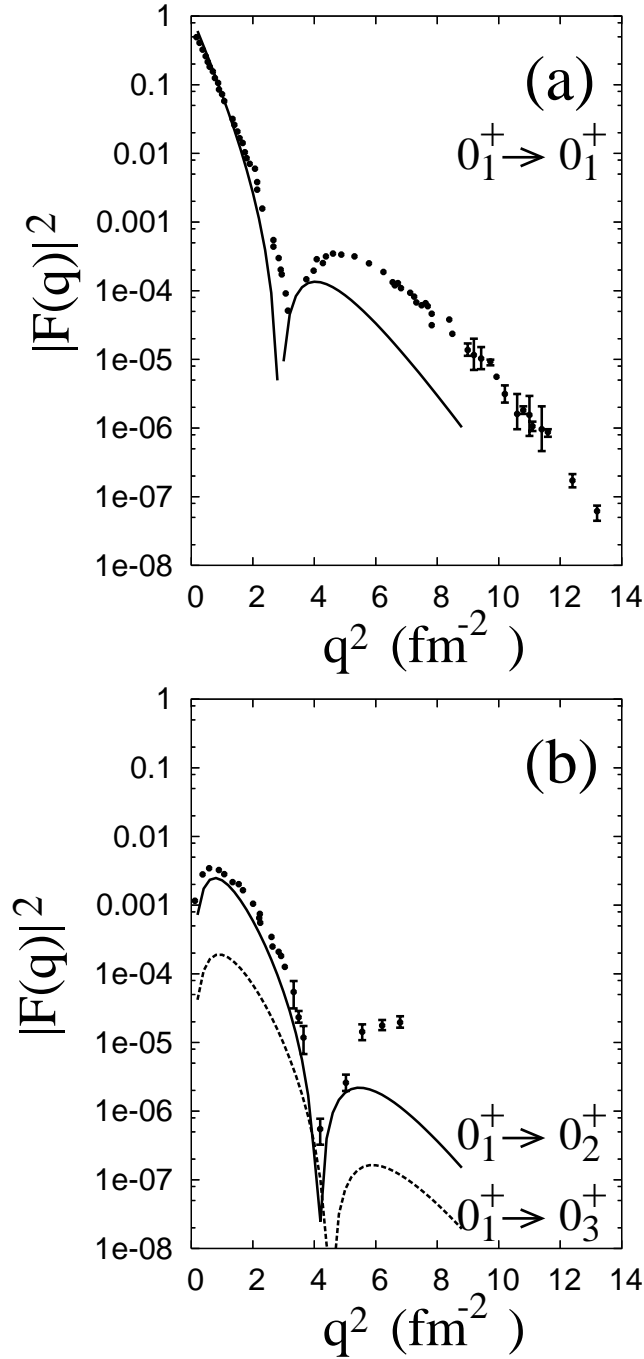


FIG. 4. Squared (a)elastic and (b)inelastic form factors of the electron scattering from ^{12}C given by the calculated transition densities and by the observation [33].

TABLE III. Calculated $\log ft$ values of the Gamov-Teller transitions for β^+ decays compared with the experimental data for $^{12}\text{N}(\beta^+)^{12}\text{C}^*$ taken from Ref. [32].

Excitation energy (MeV)	Exp.		Theory(AMD)	
	J_f^π	$\log ft$	J_f^π	$\log ft$
0	0^+	4.118 ± 0.003	3.8	0_1^+
4.44	2^+	5.149 ± 0.008	4.8	2_1^+
7.65	0^+	4.34 ± 0.07	4.3	0_2^+
10.3	(0^+)	4.36 ± 0.18	4.7	0_3^+
12.71	1^+	3.51 ± 0.17	3.7	
			6.3	2_2^+
			5.0	2_3^+

D. GT and M1 transitions

The β decay strengths from neighboring nuclei, ^{12}B and ^{12}N to the ground and excited states of ^{12}C are experimentally known. The observed values are of great help to investigate the structure of ^{12}C as well as the electric transition strengths. However, within the 3α cluster models, it is difficult to discuss the β transitions because Gamov-Teller(GT) transition matrix for the ideal α cluster of the $(0s)^4$ configuration is exactly zero due to the Pauli principle. In other words, GT transitions to the 3α cluster component are forbidden, but the transitions are caused by the breaking of the α clusters. As a result, the β decay strengths are sensitive to the α breaking component.

In Table III, the calculated GT transition strengths for the β^+ -decay from ^{12}N are shown and compared with the experimental data. The ground state($J^\pi = 1^+$) of the parent nucleus ^{12}N is obtained with a variational calculation after spin-parity projection to the 1^+ with the width parameter $\nu = 0.19 \text{ fm}^{-2}$. The calculated strengths are in good agreement with the experimental data. The strong β decay to the ground state is because of the rather large mixing of the α breaking component, which reflects the shell-model-like feature of the j - j coupling. The GT transitions to the 0_2^+ and 0_3^+ states have significant strengths though these states are dominated by the developed 3α cluster states. The strengths of the transitions to these excited 0^+ states come from the mixing of the wave functions in the diagonalization. Before the diagonalization, it was found that the GT transitions are weak for the original single AMD wave functions, $P_{MK}^{0+} \Phi_{\text{AMD}}(\mathbf{Z}_{2,3}^{0+})$ for the 0_2^+ and 0_3^+ , where the 3α cluster structure is developed. After the diagonalization, the $P_{MK}^{0+} \Phi_{\text{AMD}}(\mathbf{Z}_1^{0+})$, $P_{MK}^{0+} \Phi_{\text{AMD}}(\mathbf{Z}_2^{0+})$ and $P_{MK}^{0+} \Phi_{\text{AMD}}(\mathbf{Z}_3^{0+})$ mix in the superposed wave functions, and the final wave functions $|0_2^+\rangle$ and $|0_3^+\rangle$ contain small fraction of the $P_{MK}^{0+} \Phi_{\text{AMD}}(\mathbf{Z}_1^{0+})$. As a result, the α breaking component, which is originally included in the ground state wave function $P_{MK}^{0+} \Phi_{\text{AMD}}(\mathbf{Z}_1^{0+})$, is contained in the $|0_2^+\rangle$ and the $|0_3^+\rangle$ through the superposition of the wave functions. This is the origin of the significant GT transitions to the 0_2^+ and the 0_3^+ . The GT transition to the 2_1^+ is weaker than that to the 0_1^+ . It is reasonable because the 3α core structure enhances in the 2_1^+ compared with the 0_1^+ as shown in the next section. The strong GT transitions to the $1_1^+(T=0)$ state at 12.71 MeV is described well by the present calculations reflecting the intrinsic spin excitation in this state.

The calculated M1 transition strengths are shown in Table IV compared with the experimental data. The results for the transitions from 1_1^+ and 1_2^+ are in good agreements with the experimental data for the $1_1^+(T=0)$ at 12.1 MeV and the $1_2^+(T=1)$ at 15.1 MeV. Therefore, we assigned the present 1_1^+ and 1_2^+ states to the observed $1_1^+(T=0)$ and $1_2^+(T=1)$ states, respectively.

V. DISCUSSIONS

A. Intrinsic structure

The present wave functions are given by the linear combination of the spin-parity eigen wave functions projected from 23 AMD wave functions $\{\Phi_{\text{AMD}}(\mathbf{Z}_n^{J^\pi})\}$. Here, $\Phi_{\text{AMD}}(\mathbf{Z}_n^{J^\pi})$ is the optimum AMD wave function, which is obtained by the VAP calculation for the J_n^π state. Since each AMD wave function is written by a single Slater determinant, it is easy to analyze its intrinsic structure. Even though those bases are superposed by the diagonalization of the Hamiltonian and norm matrices, the $\Phi_{\text{AMD}}(\mathbf{Z}_n^{J^\pi})$ is mostly the dominant component of the J_n^π state after the diagonalization. Then we firstly discuss the intrinsic structure of the $\Phi_{\text{AMD}}(\mathbf{Z}_n^{J^\pi})$. In Figure 5, we show the density distributions of the

TABLE IV. $M1$ transition strengths. The experimental data are taken from Ref. [32]. The unit is the nuclear unit, $(e\hbar/2Mc)^2$. The experimental excitation energies of the initial and final states are shown in parenthesis.

J_i^π	J_f^π	Exp.	$B(M1)$	Theory(AMD)
1_1^+ (12.1 MeV)	0_1^+ (0 MeV)	0.015 (0.002)		0.011
1_1^+ (12.1 MeV)	2_1^+ (4.4 MeV)	0.0081 (0.0014)		0.008
1_2^+ (15.1 MeV)	0_1^+ (0 MeV)	0.95 (0.02)		0.17
1_2^+ (15.1 MeV)	2_1^+ (4.4 MeV)	0.068 (0.009)		0.09
1_3^+ (15.1 MeV)	0_2^+ (7.7 MeV)	0.23 (0.04)		0.014
1_2^+ (15.1 MeV)	1_1^+ (12.1 MeV)	3.6 (1.1)		2.5

intrinsic wave functions, $\Phi_{\text{AMD}}(\mathbf{Z}_n^{J^\pi})$. As seen in Fig. 5 (a1) and (e3), the 0_1^+ and the 1^+ states have compact density distributions and no developed cluster structure. In the 2_1^+ and the 4_1^+ states of the ground band built on the 0_1^+ state, the 3α cluster core appears(Figs. 5-b1 and 5-c1). These states are considered to be the SU(3) limit 3α cluster states because the spatial development of the clustering is not remarkable. In the excited states, a variety of spatial configurations of the developed 3α cluster structure appears. The 3α in the 0_2^+ (Fig. 5-a2) has an isosceles triangle configuration which is close to an equilateral triangle. The similar configurations of the 3α are seen also in the 3_1^- , 4_1^- and 5_1^- states (Fig. 5-d3,5-e1,5-e2). In the 0_3^+ state(Fig. 5-a3), the 3α shows a rather linear-like configuration, where the largest angle of vertices is larger than 120 degree. We found such the linear-like structure also in the 2_2^+ , 6_1^+ , 1_1^- and 2_1^- . In these states, a α cluster seems almost escaping. In Fig. 5(f1)-(g3), we show the intrinsic structure obtained by the VAP with the artificial barrier potential as explained in II. Although the α particles are more confined than the case without barrier, the developed 3α cluster structures are still formed in these wave functions.

The spatial 3α configurations of the 3^- and the 1^- states in the present results are consistent with the energy minimum states in the isosceles configurations of the 3α model space [6]. On the other hand, the present configuration of the 0_2^+ state does not correspond to the energy minimum but seems to be the second minimum state in the 3α models space for the 0_2^+ [6]. After the superposition of the basis, the features of the $|0_2^+\rangle$ are similar to those of the $3\alpha\text{GCM}$ calculations, because various configurations of the 3α cluster states mix in both the present results and $3\alpha\text{GCM}$ calculations.

As explained in Sec.II, we describe the final wave functions $|J_n^\pi\rangle$ with a linear combination of the obtained wave functions, $P_{MK}^{J^\pi}\Phi_{\text{AMD}}(\mathbf{Z}_{k_i}^{J_i^\pi})$, each of which is the spin-parity eigen wave functions projected from a AMD wave function. The coefficients of Eq. 6 are determined by the diagonalization of the Hamiltonian and norm matrices with respect to all the obtained AMD states. In Table V, the amplitudes of the dominant components in the final wave functions $|J_n^\pi\rangle$ are listed. In many cases, the dominant component in the $|J_n^\pi\rangle$ is the $P_{MK}^{J^\pi}\Phi_{\text{AMD}}(\mathbf{Z}_{k_i}^{J_i^\pi})$ with $J_{ik_i}^{\pi_i} = J_n^\pi$, and therefore, the $\Phi_{\text{AMD}}(\mathbf{Z}_n^{J^\pi})$ is regarded as the approximate intrinsic state of the J_n^π state.

The $|0_1^+\rangle$, $|2_1^+\rangle$ and $|4_1^+\rangle$ in the ground band contain about 90% component of the dominant $P_{MK}^{J^\pi}\Phi_{\text{AMD}}(\mathbf{Z}_k^{J^\pi})$. In the 3α cluster states, the amplitudes of the dominant component decrease mainly due to the mixing of various 3α configurations. Especially, in the $|0_2^+\rangle$, the amplitude of the $P_{00}^{0^+}\Phi_{\text{AMD}}(\mathbf{Z}_2^{0^+})$ is only 0.49, and it contains other 3α configurations such as $P_{00}^{0^+}\Phi_{\text{AMD}}(\mathbf{Z}_3^{2^+})$. The mixing of the different 3α configurations in the $|0_2^+\rangle$ enhances the loosely binding nature of the 3α particles, and increases the S -wave component of the ${}^8\text{Be}(0^+)$ - α motion. On the other hand, the dominant amplitude in the $|3_1^- \rangle$ is 0.82, which is large compared with other 3α cluster states. It may indicate that this state still has a nature of the rigid structure of the triangular 3α configuration. The intrinsic state of the dominant component in the $|4_2^+\rangle$ and $|6_1^+\rangle$ is $\Phi_{\text{AMD}}(\mathbf{Z}_1^{6^+})$, where an α particle is almost escaping and locates at the distance $r \sim 7$ fm. Their stability against α decays should be carefully discussed to confirm the possible existence of these states. Since the $|2_3^+\rangle$ is dominated by $P_{MK}^{J^\pi}\Phi_{\text{AMD}}(\mathbf{Z}_{k_i}^{J_i^\pi})$ with $J_{ik_i}^{\pi_i} = 2_3^+$ and $K = 2$, this state is considered to be the band head state of a side-band $K^\pi = 2^+$. In the negative parity states, the intrinsic structures of the $\Phi_{\text{AMD}}(\mathbf{Z}_k^{J^\pi})$'s with $J_k^\pi = 3_1^-, 4_1^-, 5_1^-$ are similar to each other, and they construct the $K^\pi = 3^-$ band; $\{3_1^-, 4_1^-, 5_2^-\}$. On the other hand, the $\Phi_{\text{AMD}}(\mathbf{Z}_k^{J^\pi})$'s for $J_k^\pi = 1_1^-$ and $J_k^\pi = 2_1^-$ have almost the same linear-like structures and form the $K^\pi = 1^-$ band, $\{1_1^-, 2_1^-, 3_2^-, 4_2^-, 5_1^-\}$. These negative parity bands, $K^\pi = 3^-$ and $K^\pi = 1^-$ were suggested also in $3\alpha\text{GCM}$ calculations.

In Table VI, we show the expectation values of the total spin(\mathbf{J}), the intrinsic spin(\mathbf{S}), the angular-momentum(\mathbf{L}), and the principal quanta of harmonic oscillator(N^{ho}) for the spin-parity projected states $P_{MK}^{J^\pi}\Phi_{\text{AMD}}(\mathbf{Z}_k^{J^\pi})$. Here, the oscillator quanta N^{ho} is defined as,

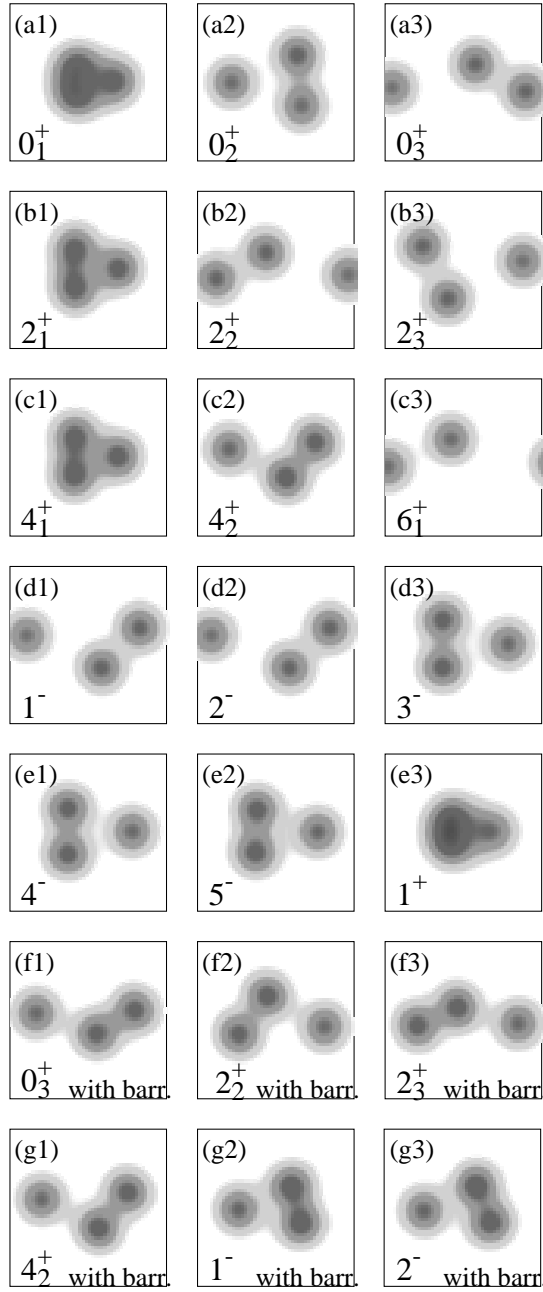


FIG. 5. Mass density distributions of the intrinsic state $\Phi_{\text{AMD}}(\mathbf{Z}_n^{J\pi})$ before the projection for the states obtained by the VAP calculations with respect to the J_n^π . Figures (f1)-(g3) are the mass density distributions of the states obtained with the artificial potential barrier. The intrinsic system is projected onto a plane which contains the major axis of the intrinsic state. The density is integrated along a transverse axis perpendicular to the plane. The size of the frame box is $10 \text{ fm} \times 10 \text{ fm}$.

TABLE V. Overlap between $P_{MK}^{J\pi}\Phi_{\text{AMD}}(\mathbf{Z}_k^{J\pi})$ and the final wave functions $|J_n^\pi\rangle$. The $|J_n^\pi\rangle$ is obtained by linear combination of $P_{MK}^{J\pi}\Phi_{\text{AMD}}(\mathbf{Z}_{k_i}^{J_i\pi_i})$ as explained in Eq. 6. K is taken to be the same value as chosen in the VAP calculations. The overlap with the largest component in the $|J_n^\pi\rangle$ is also shown in case that the overlap with other components is larger than $|\langle J_n^\pi | P_{MK}^{J\pi}\Phi_{\text{AMD}}(\mathbf{Z}_n^{J\pi}) \rangle|^2$.

after diagonalization	before diagonalization	overlap	overlap with the largest component
J_n^π	J_k^π, K	$ \langle J_n^\pi P_{MK}^{J\pi}\Phi_{\text{AMD}}(\mathbf{Z}_k^{J\pi}) \rangle ^2$	
$\langle 0_1^+ $	$0_1^+, 0$	0.89	
$\langle 0_2^+ $	$0_2^+, 0$	0.49	$ \langle 0_2^+ P_{00}^{0+}\Phi_{\text{AMD}}(\mathbf{Z}_{k=3}^{2+}) \rangle ^2 = 0.62$
$\langle 0_3^+ $	$0_3^+, 0$	0.63	
$\langle 1_1^+ $	$1_1^+, 0$	0.79	
$\langle 2_1^+ $	$2_1^+, 0$	0.91	
$\langle 2_2^+ $	$2_2^+, 0$	0.70	
$\langle 2_3^+ $	$2_3^+, 0$	0.17	$ \langle 2_3^+ P_{02}^{2+}\Phi_{\text{AMD}}(\mathbf{Z}_{k=3}^{2+}) \rangle ^2 = 0.51$
$\langle 2_4^+ $	$2_3^+, 0$	0.27	$ \langle 2_4^+ P_{00}^{2+}\Phi_{\text{AMD}}(\mathbf{Z}_{k=2}^{2+}; \text{barrier}) \rangle ^2 = 0.30$
$\langle 4_1^+ $	$4_1^+, 0$	0.90	
$\langle 4_2^+ $	$4_2^+, 0$	0.13	$ \langle 4_2^+ P_{00}^{4+}\Phi_{\text{AMD}}(\mathbf{Z}_{k=1}^{6+}) \rangle ^2 = 0.47$
$\langle 6_1^+ $	$6_1^+, 0$	0.57	$ \langle 6_1^+ P_{00}^{6+}\Phi_{\text{AMD}}(\mathbf{Z}_{k=2}^{2+}) \rangle ^2 = 0.70$
$\langle 1_1^- $	$1_1^-, 1$	0.74	
$\langle 2_1^- $	$2_1^-, 1$	0.72	$ \langle 2_1^- P_{0,-1}^{2-}\Phi_{\text{AMD}}(\mathbf{Z}_{k=1}^{1-}) \rangle ^2 = 0.79$
$\langle 3_1^- $	$3_1^-, 3$	0.82	
$\langle 3_2^- $	$3_1^-, 3$	0.10	$ \langle 3_2^- P_{01}^{3-}\Phi_{\text{AMD}}(\mathbf{Z}_{k=1}^{2-}) \rangle ^2 = 0.69$
$\langle 4_1^- $	$4_1^-, 3$	0.72	
$\langle 4_2^- $	$4_1^-, 3$	0.26	$ \langle 4_2^- P_{01}^{4-}\Phi_{\text{AMD}}(\mathbf{Z}_{k=1}^{2-}) \rangle ^2 = 0.59$
$\langle 5_1^- $	$5_1^-, 3$	0.18	$ \langle 5_1^- P_{01}^{5-}\Phi_{\text{AMD}}(\mathbf{Z}_{k=1}^{1-}) \rangle ^2 = 0.77$
$\langle 5_2^- $	$5_1^-, 3$	0.76	

$$N^{\text{ho}} \equiv \sum_i \left[\frac{\mathbf{P}_i^2}{4\hbar^2\nu} + \nu\mathbf{r}_i^2 - \frac{3}{2} \right], \quad (8)$$

where the width parameter ν is chosen to be the same value as that of the single-particle Gaussian wave packets. We also show the expectation values of those operators for the final wave functions $|J_n^\pi\rangle$ after the diagonalization in Table VII.

Non-zero values of the intrinsic spins indicate the breaking of 3α clustering. Due to the 3α cluster structure, the $\langle \mathbf{S}^2 \rangle$ values are almost zero in many states before the diagonalization except for the 0_1^+ and 1_1^+ states as seen in Table VI. The origin of the non-zero $\langle \mathbf{S}^2 \rangle$ in the 0_1^+ state is the mixing of the $p_{3/2}$ sub-shell closure component. In case of the 1_1^+ state, non-zero $\langle \mathbf{S}^2 \rangle$ originates in the intrinsic spin excitation. More detailed discussions of the α -cluster breaking is given later.

The proton total spin $\langle \mathbf{J}_p^2 \rangle$ and neutron total spin $\langle \mathbf{J}_n^2 \rangle$ are the smallest in the 0_1^+ state. It is because of the significant $p_{3/2}$ sub-shell closure component. On the other hand, they are quite large in the 0_2^+ and the 0_3^+ states compared with the 0_1^+ . This comes from the component of the orbital-angular momenta $L_p \neq 0$ and $L_n \neq 0$, which are caused by the strong correlations of nucleons in the developed α clusters. In case of the 0_2^+ state, those values becomes larger in the $|0_2^+\rangle$ after the diagonalization of the basis than those in the $P_{00}^{0+}\Phi_{\text{AMD}}(\mathbf{Z}_2^{0+})$ before the diagonalization. It indicates that the further developed 3α configurations mix in the $|0_2^+\rangle$ through the superposition of the basis.

The oscillator quanta N^{ho} is equivalent to the principal quantum number of the spherical harmonic oscillator with the oscillation number $\omega = 2\hbar\nu/m$ (m is the nucleon mass), and its expectation value indicates how large the mixing of higher shell components is in the expansion of spherical harmonic oscillator basis. In the ground band members, 0_1^+ , 2_1^+ , 4_1^+ states, the values of the oscillator quanta for protons ($\langle N_p^{\text{ho}} \rangle$) and neutrons ($\langle N_n^{\text{ho}} \rangle$) nearly equal to the minimum value 4, which correspond to the $0\hbar\omega$ states. On the other hand, those for the spatially developed 3α cluster states such as the 0_2^+ , 0_3^+ , 1_1^- and 3_1^- are much larger than 4. These cluster states should be written by linear combinations of a large number of the higher shell configurations in the expansion of the harmonic oscillator basis. Therefore, it is natural that these cluster states can not be described even by the large-basis shell model calculations [3].

TABLE VI. Expectation values of the squared total spin(\mathbf{J}^2), the squared intrinsic spin(\mathbf{S}^2), the squared angular-momentum(\mathbf{L}^2), and the principal quanta of harmonic oscillator(N^{ho}) for the spin-parity projected states $P_{MK}^{J\pi}\Phi_{\text{AMD}}(\mathbf{Z}_k^{J\pi})$ before the diagonalization. K is chosen to be the same value as used in the VAP calculations. The calculated values for protons($\mathbf{J}_p, \mathbf{S}_p, \mathbf{L}_p, N_p^{\text{ho}}$), neutrons($\mathbf{J}_n, \mathbf{S}_n, \mathbf{L}_n, N_n^{\text{ho}}$), and the total system(\mathbf{S}, \mathbf{L}) are shown.

J_k^π	$ K $	$\langle \mathbf{J}_p^2 \rangle$	$\langle \mathbf{J}_n^2 \rangle$	$\langle \mathbf{S}^2 \rangle$	$\langle \mathbf{S}_p^2 \rangle$	$\langle \mathbf{S}_n^2 \rangle$	$\langle \mathbf{L}^2 \rangle$	$\langle \mathbf{L}_p^2 \rangle$	$\langle \mathbf{L}_n^2 \rangle$	$\langle N_p^{\text{ho}} \rangle$	$\langle N_n^{\text{ho}} \rangle$
0_1^+	0	0.8	0.8	1.6	0.8	0.8	1.6	1.5	1.5	4.1	4.1
0_2^+	0	6.5	6.5	0.1	0.0	0.0	0.1	6.5	6.5	6.6	6.5
0_3^+	0	15.1	15.1	0.0	0.0	0.0	0.0	15.1	15.1	14.3	14.3
1_1^+	0	2.3	0.9	3.4	2.0	1.0	3.6	2.3	1.6	4.3	4.1
2_1^+	0	4.3	4.2	0.6	0.3	0.3	6.2	4.3	4.3	4.4	4.4
2_2^+	0	16.2	16.2	0.0	0.0	0.0	6.0	16.2	16.2	14.1	14.0
2_3^+	0	12.3	12.3	0.0	0.0	0.0	6.2	12.3	12.3	10.4	10.3
4_1^+	0	7.2	7.1	0.3	0.1	0.1	19.3	7.0	6.9	4.5	4.5
4_2^+	0	12.8	12.8	0.1	0.0	0.0	20.0	12.8	12.8	7.6	7.6
1_1^-	1	11.9	11.9	0.0	0.0	0.0	2.0	11.9	11.9	11.3	11.2
2_1^-	1	13.9	13.9	0.0	0.0	0.0	6.0	13.9	13.9	12.4	12.3
3_1^-	3	9.7	9.7	0.1	0.0	0.1	12.0	9.7	9.6	6.4	6.3
4_1^-	3	11.3	12.0	0.1	0.0	0.0	19.9	11.3	11.1	6.3	6.3

TABLE VII. Expectation values of the squared total spin(\mathbf{J}^2), the squared intrinsic spin(\mathbf{S}^2), the squared angular-momentum(\mathbf{L}^2), and the principal quanta of harmonic oscillator(N^{ho}) for the final wave functions $|J_k^\pi\rangle$ obtained by the superposition of the wave functions after the diagonalization. The calculated values for protons($\mathbf{J}_p, \mathbf{S}_p, \mathbf{L}_p, N_p^{\text{ho}}$), neutrons($\mathbf{J}_n, \mathbf{S}_n, \mathbf{L}_n, N_n^{\text{ho}}$), and the total system(\mathbf{S}, \mathbf{L}) are shown.

$ J_k^\pi\rangle$	$\langle \mathbf{J}_p^2 \rangle$	$\langle \mathbf{J}_n^2 \rangle$	$\langle \mathbf{S}^2 \rangle$	$\langle \mathbf{S}_p^2 \rangle$	$\langle \mathbf{S}_n^2 \rangle$	$\langle \mathbf{L}^2 \rangle$	$\langle \mathbf{L}_p^2 \rangle$	$\langle \mathbf{L}_n^2 \rangle$	$\langle N_p^{\text{ho}} \rangle$	$\langle N_n^{\text{ho}} \rangle$
0_1^+	1.7	1.7	1.2	0.6	0.6	1.2	2.2	2.2	4.4	4.4
0_2^+	8.0	8.0	0.6	0.3	0.3	0.6	8.3	8.3	8.4	8.3
0_3^+	14.4	14.4	0.2	0.1	0.1	0.2	14.5	14.5	14.0	13.9
1_1^+	1.8	1.5	3.9	1.6	1.4	4.0	2.1	1.9	4.2	4.2
1_2^+	1.5	1.9	2.2	1.3	1.5	2.3	1.8	2.0	4.2	4.2
2_1^+	4.7	5.0	0.5	0.3	0.2	6.1	4.7	5.0	4.8	4.8
2_2^+	16.1	16.1	0.0	0.0	0.0	6.0	16.1	16.1	13.9	13.9
2_3^+	11.3	11.8	0.3	0.2	0.1	6.0	11.3	11.7	10.1	10.1
2_4^+	15.0	15.0	0.1	0.0	0.0	6.0	15.0	15.0	13.0	12.9
4_1^+	8.0	8.1	0.2	0.1	0.1	19.5	7.9	8.0	5.1	5.1
4_2^+	21.2	21.3	0.0	0.0	0.0	20.0	21.2	21.3	15.5	15.4
1_1^-	9.8	9.9	0.1	0.0	0.0	2.1	9.8	9.9	9.4	9.3
2_1^-	11.4	11.4	0.1	0.0	0.0	6.0	11.4	11.4	9.9	9.8
3_1^-	10.8	10.6	0.1	0.1	0.1	12.0	10.8	10.5	7.4	7.3
3_2^-	14.1	14.1	0.1	0.1	0.1	12.0	14.0	14.1	10.9	10.8
4_1^-	13.0	12.9	0.1	0.0	0.1	19.9	13.0	12.9	7.9	7.8
4_2^-	15.3	15.4	0.1	0.0	0.0	20.0	15.3	15.4	10.4	10.3

B. Breaking of α clusters

In the present framework, the existence of α clusters is not assumed, but the formation and breaking of the clusters are automatically incorporated in the energy variation if such the structures are favored. We can estimate the α breaking components with the non-zero values of the squared intrinsic spins, $\langle \mathbf{S}^2 \rangle$, listed in Table VI and VII.

Let us first discuss the cluster and non-cluster components in the wave functions by analyzing the results shown in Table VI before the diagonalization. The states except for the 0_1^+ , 2_1^+ , 4_1^+ and 1_1^+ have almost zero values of $\langle \mathbf{S}^2 \rangle$ because of the well-developed 3α cluster structures. It means that the α clusters are not broken in these cluster states. On the other hand, $\langle \mathbf{S}^2 \rangle = 1.6$ in the 0_1^+ state indicates the significant α breaking component. It is natural because $p_{3/2}$ sub-shell closed configuration is favored in the ground state. If the ground state is the pure $p_{3/2}$ sub-shell closed state, the expectation values of the squared total spins for protons ($\langle \mathbf{J}_p^2 \rangle$) and neutrons ($\langle \mathbf{J}_n^2 \rangle$) should be zero. Considering the non-zero values ($\langle \mathbf{J}_p^2 \rangle = \langle \mathbf{J}_n^2 \rangle = 0.8$), the 0_1^+ state is considered to be a mixture of the $SU(3)$ -limit 3α state and the $p_{3/2}$ -shell closed state. In other words, the 3α clustering is partially broken due to the spin-orbit force in the ground state. The 1^+ is the non 3α state with intrinsic spin excitations as seen in its spin magnitude ($\langle \mathbf{S}^2 \rangle = 3.4$). It is consistent with the fact that the $J^\pi = 1^+$ is unnatural in a 3α system.

Next we look into the α breaking in the $|J_n^\pi\rangle$ after the diagonalization. By comparing the values in Table VII with those in Table VI, we found that the α breaking component in the original wave function of the ground state mixes into the $|0_2^+\rangle$ and $|0_3^+\rangle$ because the $\langle \mathbf{S}^2 \rangle$ values of the $|0_2^+\rangle$ and $|0_3^+\rangle$ become large due to the diagonalization. In the 0_2^+ state, the angular momentum $\langle \mathbf{L}_{p(n)}^2 \rangle$ for protons(neutrons) increases as well as the intrinsic spins $\langle \mathbf{S}^2 \rangle$ due to the superposition of the wave functions. It indicates that not only the α -breaking component but also the component of further developed 3α clustering increases in the 0_2^+ state through the diagonalization.

As mentioned before, the GT transition strengths are good probes to investigate the mixing of cluster and non-cluster components, because the transitions to the ideal 3α cluster states are forbidden, and therefore, the strengths directly reflect the α breaking component. In the experimental observations, β decays from ^{12}N to the ground state of ^{12}C are rather strong as shown in Table III. Even for the transitions to the excited states, 0_2^+ and 0_3^+ , the significant strengths of the β decays were observed. These facts indicate that the α breaking component is contained in the 0_2^+ and 0_3^+ states as well as the 0_1^+ state. In the present study, we found that the α breaking is significantly included in the original 0_1^+ wave function due to the spin-orbit force, while the original 0_2^+ and 0_3^+ wave functions before the diagonalization have the well-developed 3α structure but no α breaking. When we calculated the GT transitions for the original wave functions before the superposition of the basis, we obtained almost forbidden GT transitions into the 0_2^+ and 0_3^+ states because of the 3α cluster structures, and failed to reproduce the experimental $\log ft$ values. The α breaking components are slightly contained in the $|0_2^+\rangle$ and $|0_3^+\rangle$ after the diagonalization through the mixing of the original 0_1^+ wave function, which includes the $p_{3/2}$ sub-shell closed configuration. As a result of the mixing of the α breaking components, the $\log ft$ values are well reproduced by the present wave functions after the diagonalization.

The α breaking gives important effects on various properties of the ground and excited states of ^{12}C as well as the GT transition strengths. As mentioned before, the level spacing between the 0_1^+ and 2_1^+ states is as large as the experimental data because the ground state gains the spin-orbit force due to the α breaking. This large level spacing can not be described by the 3α cluster models. The α breaking component of the ground state should affect also the properties of the excited 0^+ states. Within the 3α model space, the ground state is almost the $SU(3)$ -limit 3α state, while the excited 0_2^+ state is an optimum solution in the model space orthogonal to the 3α ground state. It means that the compact 3α state is forbidden for the 0_2^+ state to satisfy the orthogonality to the ground state. In the present work, since the ground state contains the α breaking component, the $SU(3)$ -limit 3α state is partially allowed for the 0_2^+ state. We consider that this is one of the reasons for the smaller radius of the 0_2^+ state in the present calculations than the values obtained by the 3α calculations. The reduction of the 0_2^+ size due to the non- 3α component in the ground state should be important also in the description of the experimental value of the $E2$ strength. The experimental data of $B(E2; 0_2^+ \rightarrow 2_1^+)$ is usually underestimated by the 3α calculations. In the present study, we can describe the increase of $B(E2; 0_2^+ \rightarrow 2_1^+)$ by the effect of the size reduction, which enlarges the overlap of the 0_2^+ with the 2_1^+ . Since the present $B(E2; 0_2^+ \rightarrow 2_1^+)$ value is larger than the experimental one, the effect of the α breaking might be overestimated.

Let us discuss the α breaking effect on the inelastic form factor to the 0_2^+ state. Funaki *et al.* showed that the maximum value of the inelastic form factor is sensitive to the spatial extension of the 0_2^+ state. In their analysis based on the 3α condensate wave function, the magnitude of the form factor decreases with the enhancement of the 0_2^+ size. They succeeded to reproduce the experimental data of the inelastic form factor by the 3α condensate wave function with a large radius $R_m = 3.8$ fm. On the other hand, as shown in Fig. 4, the present results well reproduce the maximum value of the form factor, though the root-mean-square radius of the 0_2^+ is $R_m = 3.3$ fm which is smaller than that of their calculations. The $E0$ strengths should be sensitive also to the structure of the ground state. If the ground state contains the α breaking component, the inelastic transition strength to the excited 3α state should

TABLE VIII. The calculated reduced α -decay widths(θ^2), the amplitudes ($ry_L(r)$), S factors, cluster probabilities, α -decay widths for the ${}^8\text{Be}(0^+)+\alpha$ channel. The assumed excitation energies E_x for the 0_3^+ and the 2_2^+ states are shown in parenthesis. The calculated α decay widths are obtained with the experimental energy E_α of the relative motion between ${}^8\text{Be}(0^+)$ and α . The experimental widths [32] are also shown.

J^π	$E_x(\text{MeV})$	E_α	channel radius		reduced width		S -factor	Cluster probability	$\Gamma_{\text{cal}}(\text{keV})$	$\Gamma_{\text{exp}}(\text{keV})$
			$a(\text{fm})$	$ ay(a) ^2(\text{fm}^2)$	$\theta_\alpha^2(a)$					
0_1^+	0		4.0	6.3E-02	0.08	0.31	0.43			
0_2^+	7.654	0.38	6.0	9.6E-02	0.19	0.40	0.43	0.04	8.5e-3	
0_3^+	(10.3)	(3)	7.0	6.0E-02	0.14	0.19	0.19	400	(3000)	
2_1^+	4.44		4.0	3.3E-02	0.04	0.12	0.47			
2_2^+	(10.3)	(3)	6.0	1.2E-01	0.23	0.33	0.35	460		
2_3^+			8.0	4.0E-03	0.01	0.06	0.11			
4_1^+	14.08	6.81	4.0	2.1E-02	0.03	0.08	0.52	40	258	
4_2^+			7.0	5.0E-02	0.12	0.18	0.19			

decrease, because the non- 3α component reduces the transition overlap between the ground state and the α cluster states in general. This is one of the reasons for the suppression of the inelastic transitions in the present calculations, which reproduce the magnitude of the inelastic form factor for the $0_1^+ \rightarrow 0_2^+$.

It should be stressed that the α breaking component in the ground state is directly reflected in the inelastic transition strengths from the ground state, and also can have an influence on the structure of the excited 0^+ states.

C. 3α cluster features

In many theoretical works, the 3α cluster features of ${}^{12}\text{C}$ have been discussed by many groups for a long time. Especially, the 0^+ and the 2^+ states above the 3α threshold energy have attracted great interests. Recently, there are some experimental reports on the 0^+ and 2^+ around $E_x = 10$ MeV [11–14]. However, the level structure and the assignment of these resonances have not been clarified yet. In the present work, various 3α cluster structures appear in the excited states of ${}^{12}\text{C}$. We, here, analyze the structure of the 0^+ , the 2^+ and the 4^+ states by extracting the ${}^8\text{Be}(0^+)+\alpha$ components and estimate the α decay widths with the method of reduced width amplitudes. We give a discussion of the level assignment and the band structure later in VD.

We extracted the reduced width amplitudes for the ${}^8\text{Be}(0^+)+\alpha$, and calculated the spectroscopic factors(S) and cluster probabilities. For simplicity, we assumed the $(0s)^4$ wave function for the α particle and $SU(3)$ -limit cluster wave function for the ${}^8\text{Be}(0^+)$ by using the same width parameter ν as the present AMD wave function of the ${}^{12}\text{C}$. The definitions and the detailed method of the calculations are explained in Ref. [21].

Figure 6 shows the reduced width amplitudes $ry_L(r)$ of the 0^+ , 2^+ and 4^+ states. The calculated S factors and cluster probabilities are listed in Table VIII. In the 0_1^+ , 2_1^+ and 4_1^+ states, the node numbers of the cluster wave functions are 2, 1 and 0, respectively, which correspond to the lowest allowed node numbers for the ${}^8\text{Be}-\alpha$ relative motion. In the higher J^π states, the node number increases one by one and the position of the largest peak shifts toward the large distance region. The S factors in Table VIII indicate the spatial developments of the ${}^8\text{Be}(0^+)+\alpha$ clustering. The S factor is the largest in the 0_2^+ state. Among three 2^+ states, S is the largest in the 2_2^+ state. In the 0_3^+ state, the S factor is not so large even though this state is the developed 3α cluster state. It is because the main component of the 0_3^+ is a rather linear-like 3α , which results in the reduction of the ${}^8\text{Be}(0^+)+\alpha$ component because of the large mixing of the ${}^8\text{Be}(2^+)+\alpha$ with D -wave relative motion. These behavior of the cluster wave functions $ry_L(r)$ for the 0_1^+ , 0_2^+ , 0_3^+ , 2_1^+ , 2_2^+ and 2_3^+ corresponds well to the $3\alpha\text{GCM}$ calculations by Uegaki *et al.* [6], though the present amplitudes are slightly smaller than those of the $3\alpha\text{GCM}$ results. Therefore, the basic features of the 3α cluster components in the present results are considered to be similar to those of the $3\alpha\text{GCM}$ results.

The calculated reduced widths($\theta_\alpha^2(a)$) are shown in Table VIII. The large values of $\theta_\alpha^2(a)$ in the 0_2^+ , 0_3^+ and 2_2^+ states imply the spatial development of the α cluster in these states. We estimated the ${}^8\text{Be}(0^+)+\alpha$ decay width with the method of reduced width amplitudes in the same way as in Ref. [21]. In the present estimation, we temporary assigned the 0_3^+ and the 2_2^+ to the observed states around $E_x = 10 \sim 11\text{MeV}$ and chose the energy of the relative motion E_α to be 3 MeV. The calculated α decay widths for the 0_3^+ and the 2_2^+ are 400 keV and 460 keV, respectively. In these energy region, the partial width for the ${}^8\text{Be}(0^+)+\alpha$ decay is expected to dominate the total α decay widths as shown in Ref. [6].

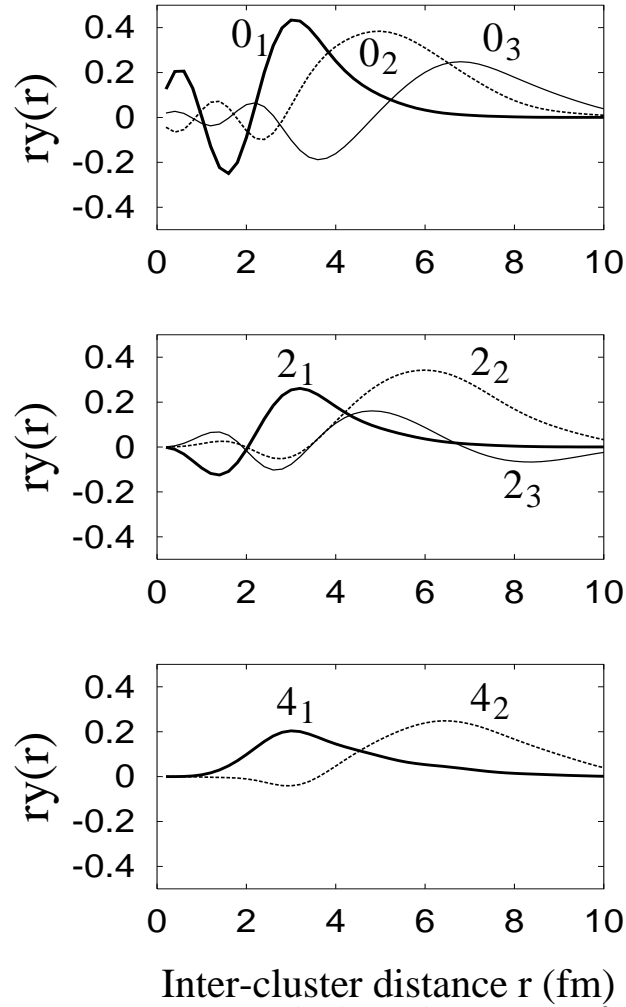


FIG. 6. α -reduced width amplitudes $ry(r)$ of the 0^+ , 2^+ and 4^+ states for the $[{}^8\text{Be}(0^+) \otimes l]_J (l = J)$ channel.

D. Assignments of 0^+ and 2^+ resonances

The 0^+ and 2^+ states around $E_x = 10$ MeV have been experimentally and theoretically studied for a long time. We here consider the correspondence of the present results with other theoretical calculations and the experimental reports.

There exists the broad resonance at $E_x = 10.3$ MeV with the width $\Gamma \sim 3$ MeV, which has been ambiguously assigned to a 0^+ state [32]. Because of the existence of this broad resonance, there remain uncertainties on the spectroscopy in this energy region. In the inelastic ${}^6\text{Li}$ and α scattering [11,31], a broad 0^+ state has been observed around $E_x = 10$ MeV. Its energy and width are consistent with the broad 0^+ at $E_x = 10.3$ MeV. The 0^+ state around $10 \sim 11$ MeV has been also observed in the recent experiments of the β -delayed 3α particle decay from ${}^{12}\text{B}$ and ${}^{12}\text{N}$ [12,14]. In the argument in [14], interference between this state and the $0_2^+(7.65$ MeV) has so significant influence on the spectrum and it makes difficult to determine the resonance energy. Recently, the 2_2^+ state has been discovered at $E_x \sim 10$ MeV by the inelastic α scattering [13]. The spectra of this state are overlapped by the broad peak of the 0^+ at 10.3 MeV, and the fitting parameter for the 2_2^+ is $E_x = 9.9 \pm 0.3$ MeV and $\Gamma = 1.0 \pm 0.3$ MeV.

The 0^+ state above the 3α threshold has been long discussed also in many theoretical studies. Morinaga *et al.* [34] proposed a linear-chain 3α structure(LCS) of the 0_2^+ at 7.65 MeV. The possibility of the LCS has been discussed based on the analysis of the α decay widths by Suzuki *et al.* [35], and it was argued that the LCS is inappropriate to explain the large experimental widths of the $0^+(7.65$ MeV) and the $0^+(10.3$ MeV). In the microscopic and semi-microscopic 3α cluster model calculations [4,6,15,36], it was found that the 0_2^+ has the developed 3α structure with the dominant $[{}^8\text{Be}(0^+) \otimes l = 0]_{J=0}$ and has the nature of the weakly interacting 3α particles. This is quantitatively consistent with the features of 3α clustering in the 0_2^+ state of the present results. Recently, the new interpretation of the 0_2^+ as a 3α -cluster gas was proposed [9,36]. Also in the present study, we found the dilute 3α gas aspects of the 0_2^+ , though its radius is somewhat smaller than that of the 3α calculations. In these theoretical studies, it is considered that the 3α structure of the 0_2^+ has been qualitatively established.

The 0_3^+ state 4 MeV above the 0_2^+ state was predicted in the $3\alpha\text{GCM}$ [6], $3\alpha\text{RGM}+\text{CSM}$ [37], and $3\alpha\text{OCM}+\text{CSM}$ [15] calculations. In the comparison with the experimental data of the $0^+(10.3$ MeV, $\Gamma_{\text{exp}}=3$ MeV), the theoretical energy is rather higher than the observed data, and the calculated width $\Gamma_{\text{cal}} \sim 1$ MeV is narrower than the $\Gamma_{\text{exp}} = 3$ MeV. Also in the present results, we obtained the 0_3^+ state a few MeV above the 0_2^+ state. The structure of this state is similar to the 0_3^+ state of the $3\alpha\text{GCM}$ calculations. As mentioned before, the dominant 3α configuration of the 0_3^+ is rather linear-like as well as the $3\alpha\text{GCM}$ calculations, where the 0_3^+ state is dominated by $[{}^8\text{Be}(2^+) \otimes l = 2]_{J=0}$ and has less $[{}^8\text{Be}(0^+) \otimes l = 0]_{J=0}$ component. This results in the suppression of the α decay width. Comparing with the observed broad width, it seems that the theoretical 0_3^+ state should not be directly assigned to the experimental $0^+(10.3$ MeV, $\Gamma_{\text{exp}}=3$ MeV). Recently, Kurokawa *et al.* predicted a new broad 0^+ resonance below the predicted 0_3^+ state. It may suggest that another broad resonance might coexist with the predicted narrower 0_3^+ state in this energy region. The possible coexistence of two 0^+ resonances in the broad 0^+ spectra at 10.3 MeV with $\Gamma_{\text{exp}} = 3$ MeV has not been experimentally excluded. By speculating the coexistence of the two 0^+ states in this energy region, we conjecture that the 0_3^+ in the present result may correspond to the narrower state of the two 0^+ resonances. There exists some experimental information concerning the total strengths of the transitions to the broad $0^+(10.3$ MeV). The inelastic ${}^6\text{Li}$ and α scattering data imply that the isoscalar monopole transition strengths to the $0^+(10.3$ MeV) is 30-100% of that to the $0^+(7.65$ MeV), while in the present results it is 10% of the strength to the 0_2^+ state. On the other hand, the calculated $B(GT)$ for the GT transition from ${}^{12}\text{N}$ to the 0_3^+ is half of the experimental strengths for the transition to the $0^+(10.3$ MeV) (see Table III). In order to clarify the properties of the 0_3^+ state, more precise experimental data and further theoretical studies are required.

Next, we discuss the 2_2^+ state. The cluster models have predicted the 2_2^+ state around $E_x = 10$ MeV as a member of the rotational band built on the 0_2^+ state [4,6,15,17]. The recent experimental report on the 2_2^+ at 9.9 ± 0.3 MeV with $\Gamma = 1.0 \pm 0.3$ [13] is consistent with the theoretical energy and width of the predicted 2_2^+ in Refs. [15,17] and also with the present results. The theoretical 2_2^+ state is dominated by $[{}^8\text{Be}(0^+) \otimes l = 2]_{J=2}$ as shown in Table VIII as well as in the 3α models [6,15,17]. Therefore, in the weak coupling picture of a ${}^8\text{Be}+\alpha$ system, the 2_2^+ state is regarded as the rotational member upon the 0_2^+ state, which has the dominant $[{}^8\text{Be}(0^+) \otimes l = 0]_{J=0}$. The $E2$ strength from the 2_2^+ to the 0_2^+ is large as $B(E2; 2_2^+ \rightarrow 0_2^+) = 100$ e^2fm^4 in the present calculations. However, by analyzing the $E2$ transitions and the intrinsic structure of the 0^+ and the 2^+ states, we can extract an alternative interpretation for the band assignment of the 2_2^+ . Namely, the 2_2^+ and the 0_3^+ can be the rotational band members of the linear-like 3α structure. In fact, we obtained the remarkably large $B(E2)$ values, $B(E2; 2_2^+ \rightarrow 0_3^+) = 310$ e^2fm^4 . Moreover, the dominant intrinsic wave functions of the 2_2^+ and the 0_3^+ are quite similar to each other. They show the linear-like 3α structure, where the largest angle of vertices of the triangle 3α configuration is larger than 120 degree (Figs. 2-a3 and 2-b2). The overlaps of the $|2_2^+\rangle$ and $|0_3^+\rangle$ with the wave function $P_{MK}^\pm \Phi_{\text{AMD}}(\mathbf{Z}_3^{0^+})$ projected from the single AMD wave function (Fig. 2-a3) are more than 60%. As a result of the similar intrinsic structure with the large deformation,

$B(E2; 2_3^+ \rightarrow 0_3^+)$ is extremely large, and the shape of the density $\rho(r)$ of these two states are quite similar to each other (Fig. 2). Consequently, in a collective picture, we consider that the 0_3^+ and the 2_2^+ states are regarded as the members of the rotational band, which is formed by the deformed intrinsic state with the linear-like 3α structure. We expect that the real 2_2^+ state may have an intermediate rotational feature of this strong coupling aspect built on the 0_3^+ state and the weak coupling one built on the 0_2^+ state. Unfortunately, the experimental information for the 2_2^+ and the 0_3^+ state is too poor to justify the band assignment of the 2_2^+ state.

VI. SUMMARY

We investigated structure of the ground and excited states of ^{12}C . The present theoretical method is based on the VAP calculations in the framework of AMD, which can describe both cluster and shell-model-like aspects. The present results systematically reproduce the various observed data such as the energy levels, electric and β transition strengths. It was found that the ground state is the mixture of the shell-model-like state and the 3α cluster state, while the developed 3α cluster structures appear in the excited states. We also obtained the 1^+ states with non- 3α cluster structure.

We discussed the α breaking components. It is important that the α breaking significantly affects not only the low-lying states but also the excited 3α cluster states. Firstly, the experimental large level spacing between the 0_1^+ and 2_1^+ states is described by the energy gain of the spin-orbit force due to the α breaking in the 0_1^+ , which contains the $p_{3/2}$ -shell closure component. It was found that the α breaking component is slightly contained even in the excited states with the developed 3α cluster structure through the mixing of the ground state wave functions with the $p_{3/2}$ -shell closure component. As a result of the mixing of the α breaking component, the significant β decay strengths are well reproduced by the present wave functions. Moreover, it is important that the non- 3α component in the ground state may change the 3α cluster structure in the excited 0^+ states through the orthogonality to the 0_1^+ state.

In the analysis of the intrinsic structure and the 3α clustering in the present results, it was found that the features of the 3α cluster components well correspond to those of the $3\alpha\text{GCM}$ calculations [6]. As well as in the $3\alpha\text{GCM}$, we obtained the 0_2^+ , 2_2^+ and 0_3^+ states. The 0_2^+ , which corresponds to the observed $0^+(7.65 \text{ MeV})$, is dominated by $[^8\text{Be}(0^+) \otimes l = 0]_{J=0}$, and shows the trend of cluster-gas features. The predicted 0_3^+ can not be directly assigned to the experimental broad 0^+ resonance (10.3 MeV). We expect that the corresponding 0^+ spectra might be overlapped by the broad $0^+(10.3 \text{ MeV})$. The predicted 2_2^+ state should be assigned to the recently observed 2^+ state at $E_x = 9.9 \text{ MeV}$ [13]. In the weak coupling picture of $^8\text{Be} + \alpha$, This 2_2^+ can be regarded as the rotational member built on the 0_2^+ state, because this state is dominated by $[^8\text{Be}(0^+) \otimes l = 2]_{J=2}$. We also proposed an alternative interpretation for the band assignment of the 2_2^+ states based on the remarkable $B(E2; 2_2^+ \rightarrow 0_3^+)$ and the similarity of the intrinsic structure with the 0_3^+ in the present results. Namely, in a collective picture, the 0_3^+ and the 2_2^+ states are considered to be the members of the rotational band, which is formed by the deformed intrinsic state with the linear-like 3α structure.

In the present work, the number of the base wave functions is limited and the 3α configurations with the large distance are not incorporated enough. Therefore, the description of the detailed resonant behavior is insufficient in the present framework. Especially, for the broad resonances with 3α clustering, the boundary conditions should be carefully treated in the calculation of the excitation energies and the widths. The broad 0^+ and 2^+ resonances have been theoretically studied with the CSM and ACCC methods in the 3α cluster models. Such methods are promising in further study on these resonances.

In conclusion, we should stress that the cluster and the shell-model-like features coexist in ^{12}C . Since these two kinds of nature interplay with each other, one should take into account both the features appropriately for a systematic study of ^{12}C . We expect that it is also significant for clarification of the properties of the 3α resonances.

ACKNOWLEDGMENTS

The author would like to thank Prof. H. Horiuchi, Prof. A. Tohsaki, Prof. P. Schuck, Dr. C. Kurokawa and Dr. Y. Funaki for many discussions. She is also thankful to members of Yukawa Institute for Theoretical Physics (YITP) in Kyoto University for valuable discussions. The computational calculations in this work were supported by the Supercomputer Projects of High Energy Accelerator Research Organization (KEK) and also the super computers of YITP. This work was supported by Japan Society for the Promotion of Science and a Grant-in-Aid for Scientific Research of the Japan Ministry of Education, Science and Culture. The work was partially performed in the ‘‘Research

REFERENCES

- [1] A. G. M. van Hees and P. W. M. Glaudemans, *Z. Phys. A* **315**, 223 (1984).
- [2] A. A. Wolters, A. G. M. van Hees, and P. W. M. Glaudemans, *Phys. Rev. C* **42**, 2053 (1990).
- [3] P. Navratil and W. E. Ormand, *Phys. Rev. C* **68**, 034305 (2003).
- [4] Y. Fukushima and M. Kamimura, *Proc. Int. Conf. on Nuclear Structure, Tokyo, 1977, edited by T. Marumori*[*J. Phys. Soc. Jpn.* **44**, 225 (1978); M. Kamimura, *Nucl. Phys.* **A351**, 456 (1981).
- [5] H. Horiuchi, *Prog. Theor. Phys.* **51**, 1266 (1974); **53**, 447 (1975)
- [6] E. Uegaki, S. Okabe, Y. Abe and H. Tanaka, *Prog. Theor. Phys.* **57**, 1262 (1977). E. Uegaki, Y. Abe, S. Okabe and H. Tanaka, *Prog. Theor. Phys.* **59**, 1031 (1978); **62**, 1621 (1979).
- [7] Y. Fujiwara *et al.*, *Prog. Theor. Phys. Suppl.***68**, 29 (1980).
- [8] P. Descouvemont and D. Baye, *Phys. Rev. C* **36**, 54 (1987).
- [9] A. Tohsaki, H. Horiuchi, P. Schuck, and G. Röpke, *Phys. Rev. Lett.* **87**, 192501 (2001).
- [10] G. Röpke, A. Schnell, P. Schuck, and P. Nozieres, *Phys. Rev. Lett.* **80**, 3177 (1998).
- [11] B. John *et al.*, *Phys. Rev. C* **68**, 14305 (2003).
- [12] H. O. U. Fynbo *et al.*, *Phys. Rev. Lett.* **91**, 082502 (2003); H. O. U. Fynbo *et al.*, *Nucl. Phys.* **A738**, 59 (2004).
- [13] M. Itoh *et al.*, *Nucl. Phys.* **A738**, 268 (2004).
- [14] C. Aa. Diget *et al.*, *Nucl. Phys.* **A760**, 3 (2005).
- [15] C. Kurokawa and K. Kato, *Nucl. Phys.* **A738**, 455 (2004).
- [16] C. Kurokawa and K. Kato, *Phys. Rev. C* **71**, 021301(R) (2005).
- [17] Y. Funaki, A. Tohsaki, H. Horiuchi, P. Schuck, and G. Röpke, *Eur. Phys. J.* **A24**, 321(2005).
- [18] Y. Funaki, H. Horiuch and A. Tohsaki, *Prog. Theor. Phys.* **115**, 115 (2006).
- [19] Y. Kanada-En'yo, *Phys. Rev. Lett.* **81**, 5291 (1998).
- [20] Y. Kanada-En'yo, H. Horiuchi and A. Doté, *Phys. Rev. C* **60**, 064304 (1999).
- [21] Y. Kanada-En'yo, H. Horiuchi *Phys. Rev. C* **68**, 014319 (2003).
- [22] N. Itagaki, S. Aoyama, S. Okabe and K. Ikeda, *Phys. Rev. C* **70**, 054307 (2004).
- [23] T. Neff and H. Feldmeier, *Nucl. Phys.* **A738**, 357 (2004).
- [24] Y. Kanada-En'yo, H. Horiuchi and A. Ono, *Phys. Rev. C* **52**, 628 (1995); Y. Kanada-En'yo and H. Horiuchi, *Phys. Rev. C* **52**, 647 (1995).
- [25] Y. Kanada-En'yo and H. Horiuchi, *Prog. Theor. Phys. Suppl.***142**, 205 (2001).
- [26] Y. Kanada-En'yo, M. Kimura and H. Horiuchi, *Comptes rendus Physique Vol.4*, 497 (2003).
- [27] T. Ando, K. Ikeda, and A. Tohsaki, *Prog. Theor. Phys.* **64**, 1608 (1980).
- [28] N. Yamaguchi, T. Kasahara, S. Nagata, and Y. Akaishi, *Prog. Theor. Phys.* **62**, 1018 (1979); R. Tamagaki, *Prog. Theor. Phys.* **39**, 91 (1968).
- [29] H. DE Vries *et al.*, *Atomic Data and Nuclear Data Tables*, **36** (1987).
- [30] Y. Funaki, A. Tohsaki, H. Horiuchi, P. Schuck, and G. Röpke, nucl-th/0601035.
- [31] W. Eyrich *et al.*, *Phys. Rev. C* **36**, 416 (1987).
- [32] F. Ajzenberg-Selove and J.H. Kelley, *Nucl. Phys.* **A506**, 1 (1990).
- [33] I. Sick and J. S. McCarthy, *Nucl. Phys.* **A150**, 631 (1970); A. Nakada, Y. Torizuka and Y. Horikawa, *Phys. Rev. Lett.* **27**, 745 (1971); and 1102 (Erratum); P. Strehl and Th. H. Schucan, *Phys. Lett.* **27B**, 641 (1968).
- [34] H. Morinaga, *Phys. Rev.* **101**, 1956 (1956); *Phys. Lett.* **21**, 78(1966).
- [35] Y. Suzuki, H. Horiuchi and K. Ikeda, *Prog. Theor. Phys.* **47**, 1517 (1972).
- [36] Y. Funaki, A. Tohsaki, H. Horiuchi, P. Schuck, and G. Röpke, *Phys. Rev. C* **67**, 051306(R) (2003).
- [37] R. Pichler, H. Oberhummer, A. Csótó and S. A. Moszkowski, *Nucl. Phys.* **A618**, 55 (1997).